Linear interference and the initiation of extratropical stratosphere-troposphere interactions

Karen L. Smith[1] and Paul J. Kushner[2]

Received 7 February 2012; revised 11 May 2012; accepted 21 May 2012; published 4 July 2012.

[1] Vertical fluxes of wave activity from the troposphere to the stratosphere correlate negatively with the Northern Annular Mode (NAM) index in the stratosphere and subsequently in the troposphere. Recent studies have shown that stratospheric NAM variability is also negatively correlated with the amplitude of the wave pattern coherent with the large-scale climatological stationary wavefield; when the climatological stationary wavefield is amplified or attenuated, the stratospheric jet correspondingly weakens or strengthens. Here we quantify the importance of this linear interference effect in initiating stratosphere-troposphere interactions by performing a decomposition of the vertical wave activity flux using reanalysis data. The interannual variability in vertical wave activity flux in both the Northern and Southern Hemisphere extratropics is dominated by linear interference of quasi-stationary waves during the season of strongest stratosphere-troposphere coupling. Composite analysis of anomalous vertical wave activity flux events reveals the significant role of linear interference and shows that "linear" and "nonlinear" events are essentially independent. Linear interference is the dominant contribution to the vertical wave activity flux anomalies preceding displacement stratospheric sudden warmings (SSWs) while split SSWs are preceded by nonlinear wave activity flux anomalies. Wave activity variability controls the timing of stratospheric final warmings, and this variability is shown to be dominated by linear interference, particularly in the Southern Hemisphere. The persistence of the linear interference component of the vertical wave activity flux, corresponding to persistent constructive or destructive interference between the wave-1 component of climatological stationary wave and the wave anomaly, may help improve wintertime extratropical predictability.

Citation: Smith, K. L., and P. J. Kushner (2012), Linear interference and the initiation of extratropical stratosphere-troposphere interactions, *J. Geophys. Res.*,*117*, D13107, doi:10.1029/2012JD017587.

1. Introduction

[2] It is well established that Northern Hemisphere (NH) extratropical zonal-mean stratospheric circulation anomalies exhibit a downward-propagating character, coupling to the troposphere on intraseasonal timescales [*Baldwin and Dunkerton*, 2001]. The associated tropospheric anomalies, which are coherent with the Northern Annular Mode (NAM), persist for over a month, suggesting that knowledge of the state of the stratosphere may improve seasonal prediction of tropospheric climate. The stratospheric anomalies themselves are initiated from the interaction between the stratospheric zonal mean flow and vertical Rossby wave activity fluxes from the troposphere to the stratosphere [*Newman et al.*, 2001; *Polvani and Waugh*, 2004; *Limpasuvan et al.*, 2004]. Interestingly, large wave anomalies in the extratropical troposphere are not always associated with enhanced vertical wave activity flux [*Nishii et al.*, 2010]. For example, most stratospheric sudden warmings (SSWs) are preceded by a blocking event yet there are many more blocking events than SSWs [*Taguchi*, 2008]. This study examines a particular wave process, termed *linear interference*, which has helped to clarify the connection between vertical wave activity fluxes and the wave anomalies themselves.

[3] Linear interference is defined to be the enhancement or attenuation of the climatological stationary wavefield by wave anomalies in interannual variability. In this report it is shown that a term related to linear interference is an important, and often a dominant, contributor to interannual variability in vertical Rossby wave activity fluxes from the troposphere to the stratosphere. The term arises from calculating wave activity flux anomalies for perturbations to a wavy background flow. Although the total wave activity flux is quadratic in the waves, wave activity flux anomalies for perturbations to a wavy background flow include contributions that are both linear and quadratic in the wave

[1]Lamont-Doherty Earth Observatory, Earth Institute at Columbia University, Palisades, New York, USA.
[2]Department of Physics, University of Toronto, Toronto, Ontario, Canada.

Corresponding author: K. L. Smith, Lamont-Doherty Earth Observatory, Earth Institute at Columbia University, 301F Oceanography, 61 Route 9W, PO Box 1000, Palisades, NY 10964-8000, USA. (ksmith@ldeo.columbia.edu)

0148-0227/12/2012JD017587

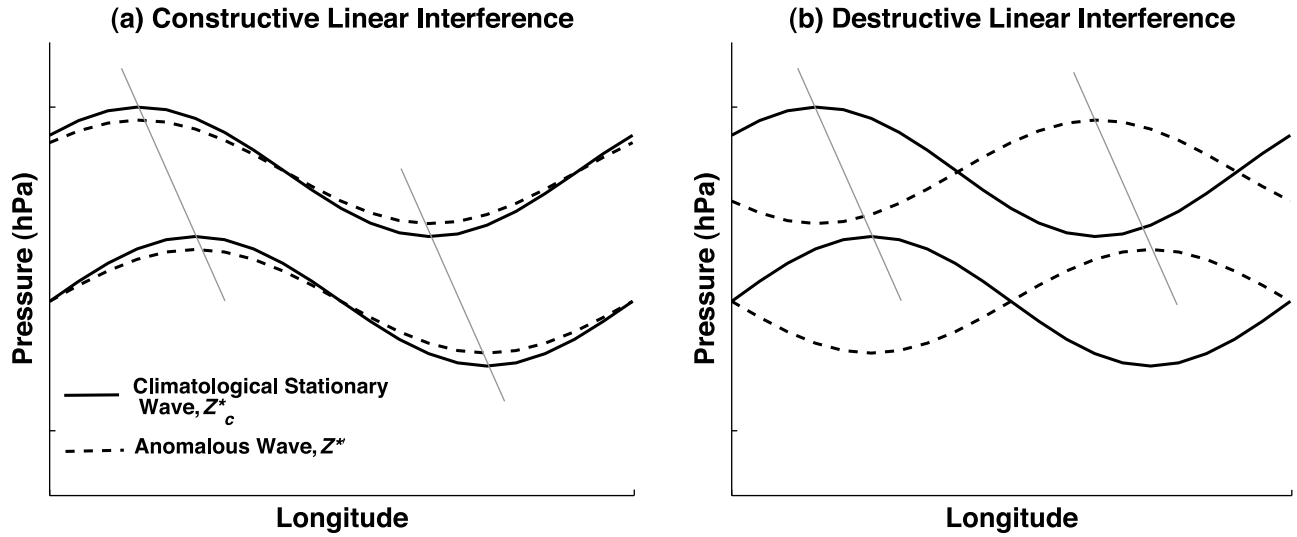

Figure 1. Schematic of (a) constructive and (b) destructive linear interference as a function of pressure and longitude. Solid and dashed black lines indicate the climatological stationary wave, Z^*_c, and the anomalous wave, $Z^{*\prime}$, respectively. The thin gray lines indicate the westward tilt of the waves.

anomalies (section 2). The linear contributions can dominate when the wave anomalies are of sufficiently small amplitude compared to the climatological stationary wave and when the wave anomalies constructively or destructively interfere with the stationary waves. There are several illustrations of linear interference in the literature [e.g., *Ineson and Scaife*, 2009, Figure 2; *Smith et al.* 2011, Figure 9]. As a summary, Figure 1 schematically illustrates constructive and destructive interference in the pressure-longitude plane. Upward-propagating Rossby wave anomalies (dashed lines) are shown to be in-phase with the climatological stationary wave (solid lines) in Figure 1a and out-of-phase in Figure 1b (the westward tilt of both the climatological stationary wave and the anomalous wave is shown by the thin gray lines).

[4] The importance of linear interference in maintaining anomalous circulation patterns in the general circulation has been previously identified [e.g., *Branstator*, 1992; *Weickmann and Sardeshmukh*, 1994; *Watanabe and Nitta*, 1998; *DeWeaver and Nigam*, 2000a]. *Branstator* [1992] finds that low-frequency variability in a perpetual winter general circulation model (GCM) simulation is maintained primarily by fluxes related to the interaction between the anomalous and climatological stationary waves. *DeWeaver and Nigam* [2000a] demonstrate that linear interference is critical in maintaining observed tropospheric zonal mean zonal wind anomalies associated with the North Atlantic Oscillation (NAO), and that there is a positive feedback between the tropospheric zonal mean and stationary wave flow components [*DeWeaver and Nigam*, 2000b].

[5] The role of linear interference in contributing to vertical wave activity flux anomalies preceding stratosphere-troposphere interactions has only recently become appreciated [*Nishii et al.*, 2009, 2010, 2011; *Garfinkel et al.*, 2010; *Kolstad and Charlton-Perez*, 2010; *Smith et al.*, 2010, 2011; *Fletcher and Kushner*, 2011]. *Nishii et al.* [2009] find that a term corresponding to the linear interference term we identify here is important for the sudden stratospheric warming of the NH in January 2006 but less important for the major warming in the Southern Hemisphere (SH) in 2002. More generally, *Garfinkel et al.* [2010] show that the variability of the NH winter stratospheric polar vortex is anti-correlated with a tropospheric wave pattern that is coherent with a small wave number approximation of the climatological stationary wavefield [see also *Kodera et al.*, 1996]. *Kolstad and Charlton-Perez* [2010] also show that a similar relationship exists in the suite of CMIP3 models. Linear interference effects have been shown to be important in linkages between the NAM and Eurasian snow cover [*Smith et al.*, 2010, 2011], ENSO and tropical variability [*Ineson and Scaife*, 2009, *Cagnazzo and Manzini*, 2009; *Fletcher and Kushner*, 2011], and blocking [*Martius et al.*, 2009; *Woollings et al.*, 2010; *Nishii et al.*, 2010, 2011].

[6] While the effects of linear interference in the coupled stratosphere-troposphere circulation have been quantified in the context of specific climate anomalies like Eurasian snow forcing and ENSO [*Smith et al.*, 2010, 2011; *Fletcher and Kushner*, 2011], a broader look at the role linear interference plays in NAM related variability is warranted. For example, these studies have shown that constructive or destructive interference tends to persist for several weeks. It is not clear whether this is a general characteristic of linear interference and what role this persistence may play in initiating stratospheric NAM events. Nor is it clear whether wave amplitude effects or wave phase structure effects dominate the variability and persistence of the wave activity flux. Finally, the characteristics and relative importance of the nonlinear contribution is unclear.

[7] This study presents a quantitative analysis of the general role of linear interference in stratosphere-troposphere interactions using *Smith et al.*'s [2011] linear/nonlinear decomposition of vertical wave activity flux anomalies that initiate stratosphere-troposphere interactions. The study will focus on the meridional wave heat flux, which is a proxy for the vertical wave activity flux. Emphasis is on the NH but comparisons are made with the SH. In section 2, the methods

will be briefly outlined. Section 3.1 describes the seasonal cycle of the meridional wave heat flux decomposition in the NH. In section 3.2 composite analysis of anomalous heat flux events in the NH is conducted with the aim of quantifying the relative importance of linear and nonlinear terms in the heat flux decomposition in stratospheric NAM variability.

[8] Stratospheric sudden warmings (SSWs) are the most dramatic and identifiable stratospheric NAM events, consisting of a reversal of the zonal mean zonal wind in the extratropical stratosphere. Recent work has systematically characterized this important phenomenon in observations and general circulation models [*Charlton and Polvani*, 2007; *Charlton et al.*, 2007; *Matthewman et al.*, 2009; *de la Torre et al.*, 2012]. In keeping with this line of work, in section 3.3, the relative importance of the linear and nonlinear heat flux anomaly terms for SSWs is established.

[9] Section 3.4 highlights the main features of linear interference and its role in stratosphere-troposphere coupling in the SH. The main issue addressed here is to what extent linear interference effects operate in the relatively weak SH stationary wavefield.

[10] Finally, in section 3.5, the role of linear interference in the timing of *stratospheric final warmings* (SFWs) in the NH and SH is discussed. SFWs characterize the breakdown of the stratospheric polar vortex during the transition from strong westerly winds in winter to weak easterly winds in the summer. They have been associated with a coupled tropospheric circulation anomaly that resembles the negative phase of the NAO [*Black et al.*, 2006]; their timing has implications for tropospheric seasonal forecasting [*Ayarzagüena and Serrano*, 2009; *Hardiman et al.*, 2011] and polar stratospheric ozone [*Salby and Callaghan*, 2007; *Hurwitz et al.*, 2010]. The issue addressed here is whether linear interference affects the timing of the westerly to easterly stratospheric wind transition at the same time as the stratospheric stationary wavefield is being suppressed.

2. Methods

[11] The characteristics of heat flux anomalies in the extratropical atmosphere are investigated using daily averaged NCEP/NCAR reanalysis from 1979 to 2009 [*Kalnay et al.*, 1996]. The analysis is limited to the modern satellite era given the improvements in the reanalysis in the SH for this time period [*Kistler et al.*, 2001]. For the SH, the year 2002, the only year on record in which a major stratospheric warming occurred, is excluded (this event is described in terms of linear interference in *Nishii et al.* [2009]). Linear trends have been removed from all time series excluding the time series used in the analysis of final warmings. The atmospheric fields of interest are the geopotential height (GPH) anomaly area-averaged over the polar cap bounded by 60°N or 60°S and standardized by its seasonally varying standard deviation, denoted $S(Z_{pcap}')$ (this field is well-correlated with the annular mode index [*Cohen et al.*, 2002; *Baldwin and Thompson*, 2009]); the wave GPH at 60°N or 60°S, Z^*, (where the superscript asterisk indicates the deviation from the zonal mean); and the zonal mean meridional wave heat flux averaged from 40 to 80°N or 40–80°S, $\{v^*T^*\}$ (braces indicating a zonal mean), which is used as a proxy for the vertical component of the wave activity flux (with a sign change in the SH). Daily, monthly and 40-day averaged heat fluxes are used (40-day averages are computed as the average over the 40 days prior to each day [*Polvani and Waugh*, 2004]). The focus is on heat fluxes at 100 hPa, i.e., wave activity fluxes from the troposphere to the stratosphere; however, all of the decompositions described below have been calculated at all vertical levels. We define, for a given day during year j,

$$v^*_j = v^{*\prime}_j + v^*_c \text{ and } T^*_j = T^{*\prime}_j + T^*_c \tag{1}$$

where the subscript j indicates the year, the subscript c indicates the climatological mean over the total number of years and the prime indicates the deviation from the climatological time mean, i.e., the anomaly. Using v^*_j and T^*_j from (1), the anomalous meridional wave heat flux can be decomposed into two components,

$$\begin{aligned}\{v^*_j T^*_j\}' &= \{v^*_j T^*_j\} - \{v^*_j T^*_j\}_c \\ &= \{v^{*\prime}_j T^{*\prime}_j\} + \{v^{*\prime}_j T^*_c\} + \{v^*_c T^{*\prime}_j\} \\ &\quad + \{v^*_c T^*_c\} - \{v^*_j T^*_j\}_c \\ &= \{v^{*\prime}_j T^{*\prime}_j\} + \{v^{*\prime}_j T^*_c\} + \{v^*_c T^{*\prime}_j\} \\ &\quad + \{v^*_c T^*_c\} - \{v^*_c T^*_c\} - \{v^{*\prime}_j T^{*\prime}_j\}_c \\ &= \text{NONLIN} + \text{LIN}\end{aligned} \tag{2}$$

where

$$\text{NONLIN} = \{v^{*\prime}_j T^{*\prime}_j\} - \{v^{*\prime}_j T^{*\prime}_j\}_c = \{v^{*\prime}_j T^{*\prime}_j\}' \text{ and}$$
$$\text{LIN} = \{v^{*\prime}_j T^*_c\} + \{v^*_c T^{*\prime}_j\}$$

[12] The climatological mean of both LIN and NONLIN is zero. Thus, LIN represents the contribution to $\{v^*_j T^*_j\}'$ involving the interference between the climatological stationary wave and the wave anomalies and is *linear* in the wave anomalies (see Figure 1) while NONLIN represents the contribution inherent to the wave anomalies themselves and is *quadratic* in the wave anomalies. Assuming that the wave anomalies are in approximate hydrostatic and geostrophic balance, NONLIN is proportional to the square of the geopotential wave amplitude (which is always positive), the zonal wave number and the vertical derivative of the phase of the geopotential wave anomaly, i.e., the baroclinic structure of the wave anomaly. This decomposition of the meridional wave heat flux provides a powerful tool for interpreting the effect of tropospheric wave anomalies on the stratospheric circulation. We have found a similar decomposition useful for interpreting extratropical circulation responses to localized perturbations in GCM simulations [*Smith et al.*, 2010; *Fletcher and Kushner*, 2011].

[13] Using equation (2), the interannual variability of $\{v^*T^*\}$ can be written as (the subscript j will be omitted for the remainder of the paper)

$$\begin{aligned}var(\{v^*T^*\}) = var(\text{LIN} + \text{NONLIN}) &= var(\text{LIN}) \\ &+ var(\text{NONLIN}) + 2cov(\text{LIN}, \text{NONLIN}).\end{aligned} \tag{3}$$

The heat fluxes can also be decomposed into high- and low-frequency wave components. The data is low-pass filtered

using an 11-day running mean. The climatological variance of the heat fluxes may be written as

$$var(\{v^*T^*\}) = var\big(\{v^*_{low}T^*_{low}\} + \{v^*_{high}T^*_{low}\} + \{v^*_{low}T^*_{high}\} + \{v^*_{high}T^*_{high}\}\big) \quad (4a)$$

$$= var(\{v^*_{low}T^*_{low}\}) + var\big(\{v^*_{high}T^*_{low}\}\big) + var\big(\{v^*_{low}T^*_{high}\}\big) + var\big(\{v^*_{high}T^*_{high}\}\big) + R, \quad (4b)$$

where R represents the series of covariance terms in the expansion of equation (4a). In addition, each of the terms in equation (4b) can be decomposed into LIN and NONLIN terms as in equation (2).

[14] Composites of anomalously positive ("HIGH") and negative ("LOW") 40-averaged $\{v^*T^*\}'$ events are generated [*Polvani and Waugh*, 2004]. Many methods for developing composites employ the selection of a threshold parameter for anomalously high and low events and a temporal separation parameter such that the same event is not counted more than once. Although such methods are commonly used, selection of the threshold and separation parameters is somewhat arbitrary. As an alternative simplified procedure, here the maximum or minimum 40-day averaged $\{v^*T^*\}'$ standardized by its seasonally varying standard deviation for each year from November–March in the NH and June–February in the SH for the years 1979–2009 is selected for the HIGH and LOW composites, respectively [*Mudryk and Kushner*, 2011]. The dates of these events are listed in Table 1. It has been verified that the results are very similar when the maximum or minimum 40-day averaged $\{v^*T^*\}'$ is selected rather than the standardized $\{v^*T^*\}'$. Standard threshold composite methods yield qualitatively similar results for a range of threshold values, but the similarity can break down for large threshold values when the number of events per composite becomes small [*Smith*, 2011, chapter 4]. The threshold method was used to construct Figure 1 of *Smith et al.* [2011], and the results found this way are similar. We also use the maximum/minimum event per year composite method to construct composites of 40-day averaged HIGH and LOW LIN and NONLIN heat flux events standardized by the seasonally varying $\{v^*T^*\}$ standard deviation (hereafter, HIGH LIN and NONLIN events, and LOW LIN and NONLIN events; see Table 1). For all the composite time series presented below from [−60, 60] days from the day of maximum or minimum heat flux anomaly, it is important to note that there is some overlap between the HIGH and LOW events. Table 1 indicates that HIGH and LOW events are generally separated by over one month in each winter, thus, the most robust characteristics of the composite time series' are illustrated in the [−30, 30] day range.

[15] For the SSW events, central SSW event dates from 1958 to 2009 are used from *Charlton and Polvani* [2007] and *Butler and Polvani* [2011]; the longer time period compared to the previous analysis is chosen to improve statistical sampling of SSWs. A central date is defined as the date when the zonal mean zonal wind at 60°N and 10 hPa becomes easterly during the season of climatological westerlies (excluding the final breakdown of the vortex in spring). There are 33 SSWs during the 1958–2009 time period. The vortex "displacement" and "split" SSW classification of *Charlton and Polvani* [2007] is used to identify 20 displacement events and 13 split events (classifications for 2002–2009 provided by Peter Hitchcock using the method of A. J. Charlton-Perez and L. M. Polvani (personal communication, 2007)). Displacement events involve displacement of the polar vortex off the pole and project primarily onto wave-1. Split events involve a stretching and split of the vortex into two (or more) distinct vortices and project primarily onto wave-2.

[16] Finally, for the analysis of stratospheric final warming (SFW) events, NH SFWs are identified as the final time that the 50-hPa zonal-mean zonal wind at 70°N drops below zero without returning to a value of 5 m s^{-1} until the following autumn [*Black and McDaniel*, 2007a], and SH SFWs are identified as the final time that the zonal mean zonal wind at 60°S drops below 10 m s^{-1} until the following austral autumn [*Black and McDaniel*, 2007b].

3. Results

3.1. Northern Hemisphere Seasonal Heat Flux Characteristics

[17] Figure 2 shows the monthly interannual $\{v^*T^*\}$ variance decomposition using equation (3). The total variance (Figure 2, black line) grows steadily over the autumn and early winter months, peaks in February, drops sharply in March, slowly decreases over the spring and summer, and reaches a minimum in July. The variance of the LIN flux anomalies is the largest contribution to the total variance from October to April (Figure 2, red line). The seasonal cycle of variance shows that the peak in the LIN variance occurs in January, coinciding with the peak in the climatological mean $\{v^*T^*\}$ (not shown), while the peak in the NONLIN variance occurs in February (Figure 2, blue line). The relative contributions of the terms in the variance decomposition (including two times the covariance term, which is negative; Figure 2, green line) result in a peak in the total variance that is one month later than the peak in the climatological mean $\{v^*T^*\}$.

[18] Notably, the covariance between the LIN and NONLIN fluxes is negative throughout most of the year except in May. The covariance is significant at the 95% level in September, November, May and July (correlations ranging from −0.45 to −0.6) and is significant at the 90% level in January and April (correlations of ∼−0.3). The variance decompositions for both the November to March averaged $\{v^*T^*\}$ and the December to February averaged $\{v^*T^*\}$ yield statistically significant correlations between LIN and NONLIN. This negative correlation may reflect interannual compensation between quasi-stationary and transient fluxes of dry static energy, which has been argued arises due to the constraints of energy conservation [*Trenberth and Stepaniak*, 2003]. We will show that in the composite mean over HIGH and LOW heat flux events, however, the LIN and NONLIN terms appear largely independent (see Figure 5).

[19] Figure 2 includes the low-frequency contributions to the $\{v^*T^*\}$ variance for LIN and NONLIN using equation (4b). The variance of LIN consists primarily of low-frequency waves (Figure 2, dashed red line). The variance of NONLIN also consists of a considerable low-frequency contribution (Figure 2, dashed blue line) but high-frequency

Table 1. Dates of the Largest Amplitude $\{v^*T^*\}'$, LIN and NONLIN Events, Separately Listed for HIGH and LOW Heat Flux Events and for the Northern Hemisphere and Southern Hemisphere[a]

	$\{v^*T^*\}'$		LIN		NONLIN	
Year	HIGH	LOW	HIGH	LOW	HIGH	LOW
			Northern Hemisphere			
1979–1980[b]	Mar. 21	Jan. 18	**Mar. 21**	Dec. 22	Dec. 19	**Jan. 27**
1980–1981	Feb. 16	Dec. 27	Nov. 1	**Dec. 31**	**Feb. 17**	Nov. 28
1981–1982	Jan. 26	Mar. 21	Jan. 6	Mar. 8	Nov. 3	Dec. 17
1982–1983	Mar. 31	Nov. 30	Jan. 4	**Nov. 30**	**Mar. 31**	Nov. 18
1983–1984[b]	Mar. 14	Feb. 4	**Mar. 10**	**Jan. 30**	Feb. 22	Dec. 19
1984–1985[b]	Jan. 5	Mar. 4	Dec. 18	**Mar. 4**	Mar. 19	Dec. 15
1985–1986	Mar. 27	Feb. 28	**Mar. 26**	Dec. 13	Dec. 2	Feb. 7
1986–1987[b]	Feb. 14	Jan. 7	**Feb. 15**	Dec. 19	Dec. 3	Mar. 18
1987–1988	Nov. 12	Jan. 26	Dec. 11	Feb. 10	Mar. 14	Dec. 31
1988–1989[b]	Mar. 13	Jan. 23	Feb. 14	Dec. 30	**Mar. 13**	**Jan. 31**
1989–1990	Feb. 12	Mar. 26	**Feb. 11**	Jan. 3	Mar. 7	Nov. 22
1990–1991	Feb. 4	Dec. 8	Mar. 31	Feb. 6	**Feb. 4**	**Dec. 7**
1991–1992	Feb. 14	Dec. 1	**Feb. 11**	**Dec. 4**	Dec. 8	Mar. 13
1992–1993	Mar. 10	Jan. 26	**Mar. 11**	**Jan. 26**	Mar. 21	Dec. 8
1993–1994	Nov. 8	Feb. 27	Jan. 2	Feb. 15	Nov. 16	Jan. 25
1994–1995	Jan. 26	Mar. 16	**Feb. 3**	Dec. 25	Dec. 23	Mar. 2
1995–1996	Mar. 31	Dec. 21	Feb. 3	**Dec. 23**	Mar. 15	Feb. 7
1996–1997	Nov. 28	Mar. 9	Dec. 22	**Mar. 4**	**Nov. 28**	Mar. 22
1997–1998	Jan. 9	Nov. 16	Mar. 31	**Nov. 14**	**Jan. 10**	Mar. 8
1998–1999[b]	Jan. 6	Jan. 30	**Jan. 5**	Feb. 12	Mar. 10	Nov. 1
1999–2000	Nov. 1	Jan. 12	**Nov. 1**	Feb. 17	**Nov. 1**	**Jan. 3**
2000–2001[b]	Feb. 19	Mar. 31	**Feb. 19**	**Mar. 31**	Dec. 10	Nov. 2
2001–2002[b]	Jan. 3	Mar. 14	Jan. 21	Mar. 24	**Jan. 3**	Nov. 26
2002–2003[b]	Jan. 24	Feb. 26	**Jan. 22**	Nov. 10	Feb. 13	**Mar. 5**
2003–2004	Nov. 11	Mar. 31	Feb. 9	**Mar. 31**	**Nov. 10**	Feb. 15
2004–2005	Mar. 26	Feb. 14	Mar. 7	Jan. 25	**Mar. 27**	Feb. 28
2005–2006[b]	Feb. 9	Mar. 15	Nov. 26	Mar. 31	Jan. 31	**Mar. 11**
2006–2007[b]	Feb. 27	Dec. 9	Nov. 1	**Dec. 10**	Dec. 15	Nov. 3
2007–2008	Nov. 3	Dec. 7	Mar. 18	Jan. 4	Feb. 19	**Dec. 2**
2008–2009[b]	Feb. 20	Mar. 23	**Feb. 21**	Nov. 1	Feb. 4	Mar. 12
			Southern Hemisphere			
1979–1980	Oct. 24	Jan. 13	Jun. 1	Dec. 3	**Oct. 18**	**Jan. 10**
1980–1981	Dec. 1	Jan. 14	Dec. 13	Sept. 17	Jul. 2	**Jan. 14**
1981–1982	Sept. 20	Nov. 1	Jan. 24	Sept. 8	**Sept. 18**	**Oct. 31**
1982–1983	Oct. 21	Dec. 1	Oct. 25	Jun. 3	Jun. 1	Jul. 14
1983–1984	Nov. 8	Dec. 18	Jul. 30	Oct. 20	Oct. 4	Jun. 15
1984–1985	Jul. 3	Feb. 1	**Jul. 4**	Dec. 21	Nov. 6	**Jan. 30**
1985–1986	Jul. 16	Jan. 16	Jun. 19	Sept. 29	**Jul. 16**	Jun. 6
1986–1987	Aug. 18	Dec. 27	Dec. 6	Oct. 27	**Aug. 18**	**Dec. 28**
1987–1988	Dec. 27	Oct. 5	Jul. 1	Nov. 25	**Dec. 27**	**Oct. 5**
1988–1989	Sept. 2	Jan. 12	Nov. 18	Jun. 26	**Sept. 2**	**Jan. 18**
1989–1990	Nov. 17	Jan. 21	**Nov. 16**	Oct. 23	**Nov. 18**	**Jan. 30**
1990–1991	Jan. 17	Nov. 6	**Jan. 14**	**Nov. 4**	Aug. 21	Jun. 1
1991–1992	Nov. 25	Jan. 4	**Nov. 22**	Aug. 6	**Nov. 25**	Jun. 5
1992–1993	Jun. 7	Dec. 9	**Jun. 10**	**Dec. 2**	Jul. 4	Aug. 25
1993–1994	Aug. 24	Oct. 11	Dec. 2	**Oct. 12**	Jul. 20	Jun. 1
1994–1995	Dec. 10	Jan. 20	Nov. 26	Oct. 7	Nov. 10	**Jan. 21**
1995–1996	Dec. 29	Oct. 26	Sept. 19	Jul. 11	**Dec. 29**	**Oct. 24**
1996–1997	Jan. 5	Nov. 5	Dec. 29	**Nov. 7**	**Jan. 14**	Dec. 6
1997–1998	Aug. 22	Oct. 26	Nov. 9	Sept. 30	Aug. 11	Nov. 11
1998–1999	Jan. 17	Nov. 28	Jul. 22	Nov. 6	**Jan. 17**	Jul. 30
1999–2000	Jan. 28	Nov. 15	Dec. 25	Jan. 24	**Jan. 28**	Dec. 3
2000–2001	Nov. 8	Feb. 24	**Nov. 12**	Jun. 18	Oct. 2	Jan. 17
2001–2002	Jan. 17	Dec. 13	Jun. 28	**Dec. 9**	**Jan. 17**	Aug. 6
2002–2003	n/a	Dec. 23	n/a	Nov. 6	n/a	**Dec. 24**
2003–2004	Nov. 4	Feb. 4	Oct. 14	Nov. 23	**Nov. 5**	Aug. 15
2004–2005	Jun. 1	Dec. 1	Aug. 19	Nov. 11	**Jun. 2**	**Dec. 5**
2005–2006	Nov. 14	Dec. 25	Sept. 26	**Jan. 2**	Jan. 8	Oct. 20
2006–2007	Jan. 23	Oct. 8	Dec. 21	Nov. 14	**Jan. 24**	Aug. 12
2007–2008	Jul. 10	Nov. 21	Oct. 22	Aug. 25	Jan. 15	Jun. 1
2008–2009	Jan. 23	Nov. 26	Jan. 1	**Nov. 22**	**Jan. 23**	Jul. 20

[a]When a given LIN or NONLIN event coincides to within 10 days of a $\{v^*T^*\}'$ event, the date is bold.

[b]Years in which a HIGH heat flux event coincides with a SSW. The dates of the HIGH heat flux events cannot be directly compared to the central dates of the SSWs of *Charlton and Polvani* [2007] and *Butler and Polvani* [2011] given the 40-day averaging of $\{v^*T^*\}'$.

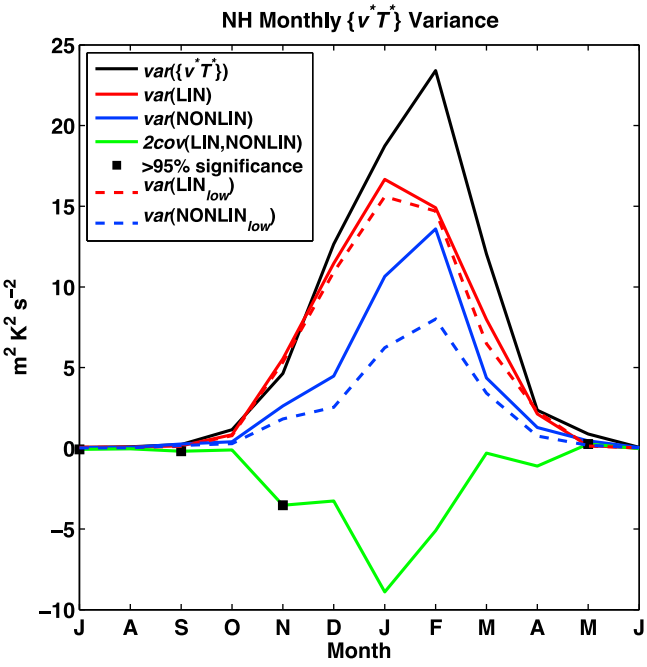

Figure 2. Monthly interannual $\{v^*T^*\}$ variance decomposition at 100 hPa averaged over 40–80°N (see equations (3) and (4b)). Subscript "low" indicates fluxes that were calculated using 11-day low-pass filtered wavefields. The black squares denote months for which the correlation between LIN and NONLIN is statistically significantly different from zero at the 95% level.

waves and the covariance between high- and low-frequency components, i.e., the R term in equation (4b), also contribute. In the winter season, the largest contribution to interannual variability in the wave activity flux, $var(\{v^*T^*\})$, is from low-frequency LIN flux anomalies.

3.2. Northern Hemisphere Anomalous Heat Flux Composites

[20] *Polvani and Waugh* [2004] demonstrate that high (low) index NAM events are highly correlated with 40-day averaged anomalously low (high) wave activity fluxes, diagnosed as meridional wave heat fluxes, in the lower stratosphere. Time–pressure composite plots of the NAM index based on heat flux anomalies are very similar to those based on NAM events themselves. Using the method outlined in section 2, 30 HIGH heat flux events (corresponding to negative NAM events) and 30 LOW heat flux (corresponding to positive NAM events) are identified. These are then composited to examine the separate contributions from the LIN and NONLIN terms.

[21] There is no significant difference in the mean timing of the HIGH and LOW heat flux composites: the mean date for HIGH heat flux events is January 28th with a standard deviation of 48 days and the mean date for LOW heat flux events is February 2nd with a standard deviation of 42 days. Table 1 shows the dates of each event for both the HIGH and LOW heat flux composites.

[22] Figures 3a–3d show the composite mean heat flux anomaly time series at 100 hPa as a function of lag (in days) and the corresponding composite mean standardized polar cap-averaged GPH anomaly, $S(Z_{pcap}')$, as a function of lag and pressure for both the HIGH and LOW heat flux composites. For HIGH heat flux events (Figure 3a) LIN fluxes are consistently larger than the NONLIN fluxes; at zero lag the LIN term is about 50% larger than the NONLIN term. The LIN flux evolves more slowly than the NONLIN flux: the LIN term increases to its peak value approximately linearly from a lag of −40 days while the NONLIN flux increases sharply near the zero lag. LIN fluxes clearly dominate LOW heat flux events (Figure 3b). The basic conclusions, that LOW heat flux events are predominantly LIN events and that HIGH heat flux events involve a mixture of LIN and NONLIN terms, are robust to the composite method used (see section 2). Consistent with *Polvani and Waugh* [2004], Figures 3c and 3d show robust negative and positive NAM-like stratosphere-troposphere coupling associated with the HIGH and LOW heat flux composites.

[23] Observed stratospheric temperature anomalies are positively skewed [*Taguchi and Yoden*, 2002], which implies that $\{v^*T^*\}'$ are likely also positively skewed. It is of interest to see how the LIN and NONLIN terms contribute to the frequency distribution of wave activity fluxes. We have calculated the distributions of the three terms in equation (2); 40-day averaged $\{v^*T^*\}'$, LIN and NONLIN at 100 hPa for the months of November to March inclusive. The distributions all have means of approximately zero. The distribution of $\{v^*T^*\}'$ is somewhat positively skewed (skew = 0.23, standard deviation = 3.1). The positive skew arises from the positive skew of the distribution of NONLIN fluxes (skew = 1.14, standard deviation = 2.1) and is consistent with large amplitude wave anomalies in the NH extratropical stratosphere having westward vertical tilt with height. The slight negative skew of the distribution of LIN fluxes (skew = −0.14, standard deviation = 2.8) partly compensates. The fact that the NONLIN contribution to the composite of the HIGH heat flux events is considerably larger than in the LOW heat flux events is consistent with the skew of the terms in the $\{v^*T^*\}'$ decomposition (Figure 3).

[24] To more clearly separate the LIN and NONLIN events, we create separate HIGH and LOW composites for anomalously positive and negative LIN and NONLIN events described in section 2 and listed in Table 1. These composites involve partially overlapping sets of events and are not independent of the HIGH and LOW heat flux composites of Figure 3. However, they are useful in that they highlight features of LIN and NONLIN events. Table 1 lists the dates for these additional composites. The HIGH LIN (Figure 4a) and NONLIN (Figure 4b) heat flux composites demonstrate the principal reason why the LIN and NONLIN fluxes are of the same sign if Figure 3 (HIGH heat flux composites in left column of Figure 3), despite the negative covariance shown in Figure 2; Figure 3a largely reflects sampling over events that consist of either predominantly LIN or predominantly NONLIN fluxes. Specifically, of the 30 HIGH heat flux events in Figure 3, 13 are also HIGH LIN events and ten are also HIGH NONLIN events (a single event that is common to both the HIGH LIN and NONLIN composites has been excluded; see Table 1). The HIGH LIN composite consists of slightly larger $\{v^*T^*\}'$ (black line) than the HIGH NONLIN composite. Figures 4a and 4b also show some evidence of the anti-correlation between LIN and NONLIN in the $\{v^*T^*\}$ variance decomposition (Figure 2).

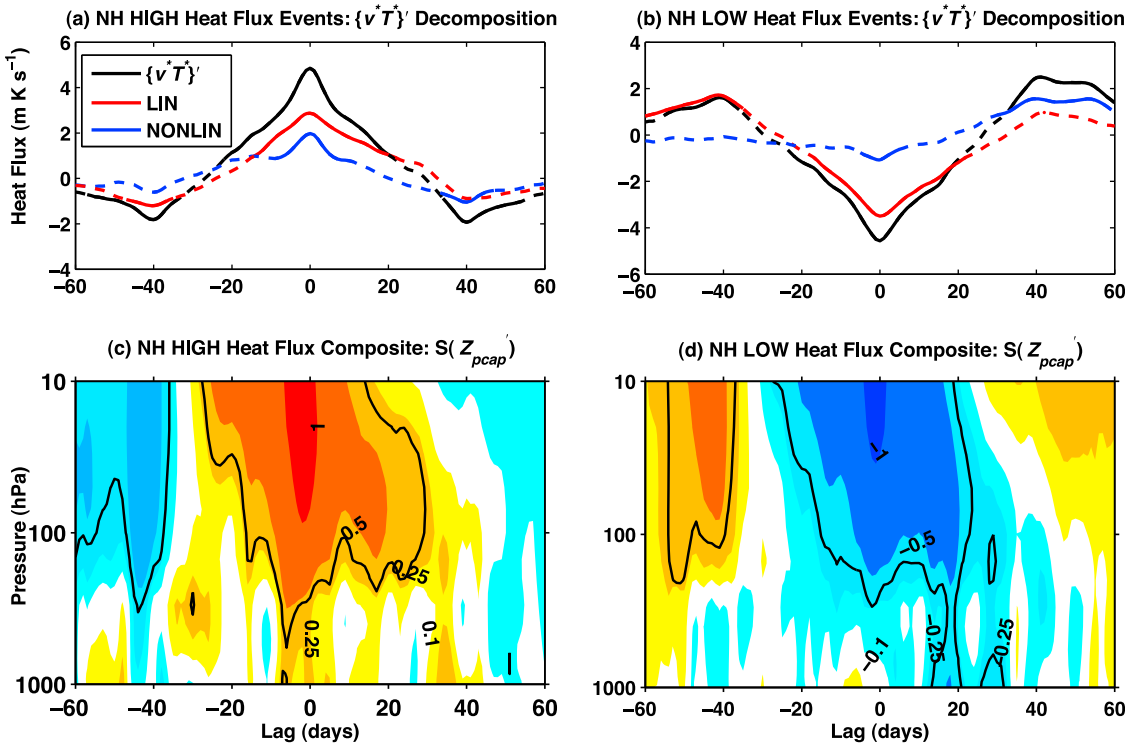

Figure 3. Composite mean 40-day averaged heat flux anomaly decomposition at 100 hPa; $\{v^*T^*\}'$ (black line), LIN (red line) and NONLIN (blue line) for NH (a) HIGH and (b) LOW heat flux events. Solid sections of the lines indicate times for which the composite mean is different from zero at the 95% significance level. Composite mean S(Z_{pcap}') for NH (c) HIGH and (d) LOW heat flux events. Contour interval is [−1.5 −1 −0.5 −0.25 −0.1 0.1 0.25 0.5 1 1.5]. Black contour indicates pressures and times for which the composite mean is different from zero at the 95% significance level.

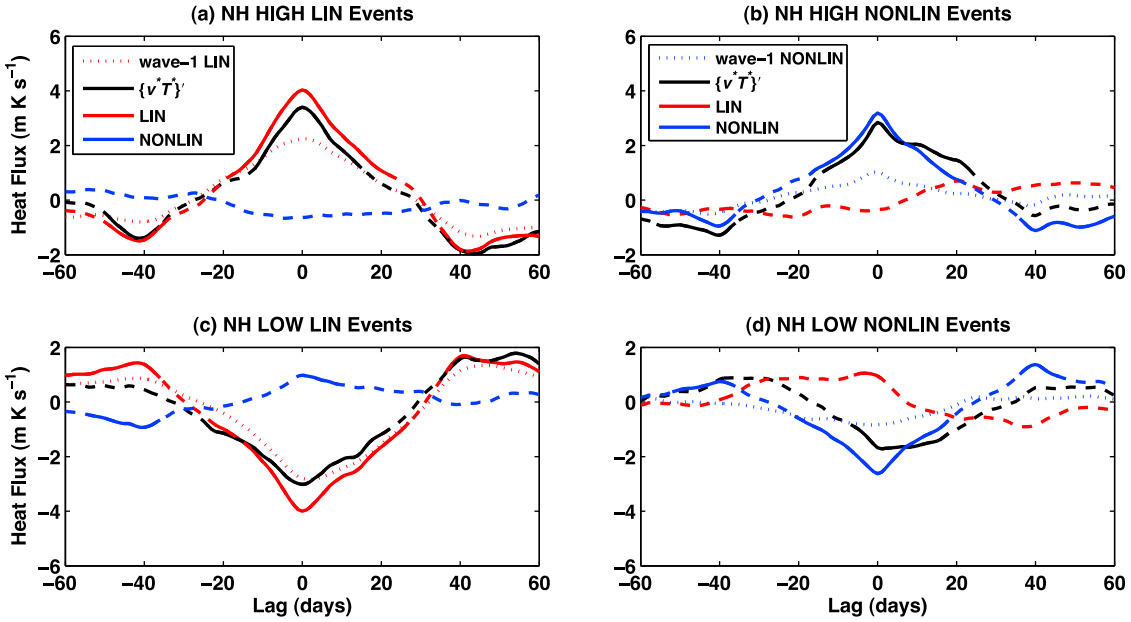

Figure 4. Composite mean 40-day averaged heat flux anomaly decomposition at 100 hPa; $\{v^*T^*\}'$ (black line), LIN (red line) and NONLIN (blue line) for HIGH (a) LIN and (b) NONLIN heat flux events. Solid sections of the lines indicate times for which the composite mean is different from zero at the 95% significance level. (c and d) same as Figures 4a and 4b but for LOW LIN and NONLIN events. The dotted lines indicate the wave-l component for LIN in Figures 4a and 4c and NONLIN in Figures 4b and 4d.

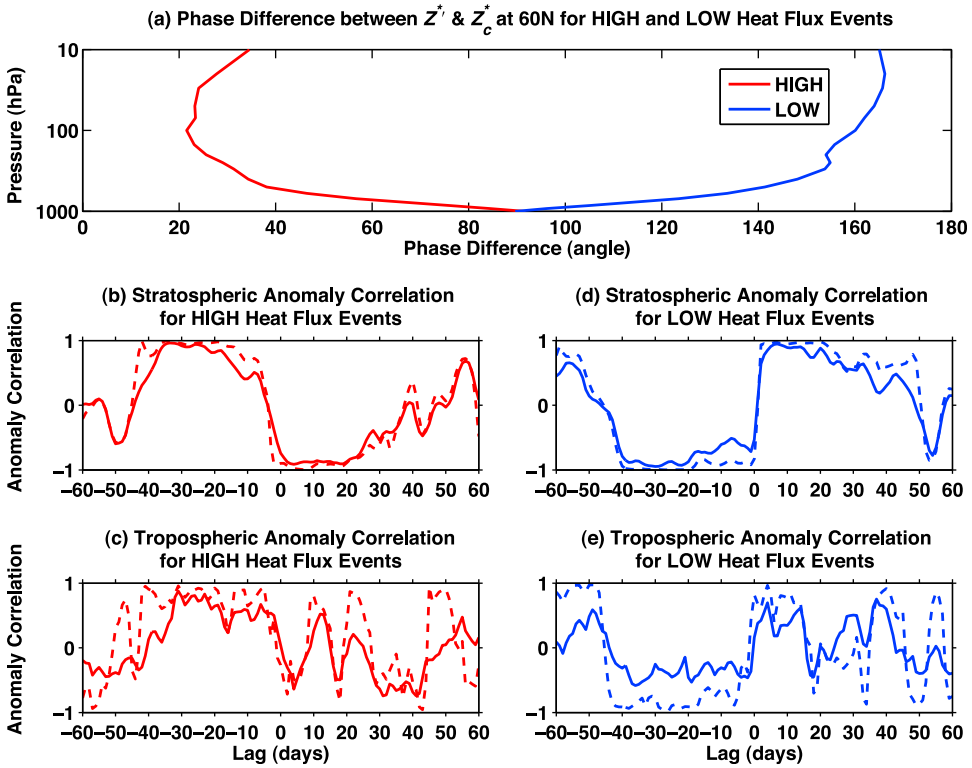

Figure 5. (a) Phase difference ($\Delta\theta$) between the composite mean $Z^{*\prime}$ and Z^{*}_{c} at 60°N averaged over days [−30, −1] for the HIGH (red line) and LOW heat flux composites (blue line). (b and d) Stratospheric anomaly correlation between the composite mean $Z^{*\prime}$ and Z^{*}_{c} at 60°N at 100 hPa for the full wave-field (solid line) and the wave-1 component (dashed line) for the HIGH and LOW heat flux composites, respectively. (c and e) Same as Figures 5b and 5d but for the tropospheric anomaly correlation.

[25] LOW LIN and NONLIN composites were also constructed (Figures 4c–4d). Of the 30 LOW heat flux events in Figure 3, 12 are LOW LIN events and seven are LOW NONLIN events. The LOW LIN and NONLIN composites show similar but opposite signed features to their HIGH counterparts in Figures 4a and 4b. The anti-correlation between LIN and NONLIN shown in Figure 2 is somewhat evident for the LOW LIN and NONLIN composites.

[26] The dotted lines in Figure 4 represent the wave-1 contribution to the LIN (red dotted line; Figures 4a and 4c) and NONLIN (blue dotted line; Figures 4b and 4d) flux anomalies. Generally, wave-1 dominates the LIN fluxes and is an important contributor to the NONLIN fluxes. Wave-2 contributes most of the remainder to both the LIN and NONLIN terms (not shown).

[27] The LIN term, which is important or dominant in all these composites, includes both a phasing effect and an amplitude effect that can be separately diagnosed. The phasing effect is illustrated in Figure 5a, which shows the wave-1 phase differences ($\Delta\theta$) between the composite mean anomalous wave GPH, $Z^{*\prime}$, and the climatological stationary wave GPH, Z^{*}_{c}, at 60°N and for days [−30, −1] for the original HIGH and LOW heat flux composite represented in Figure 3 (red and blue lines, respectively). Because $\{v^{*}T^{*}\}^{\prime}$ used to generate the composites are 40-day averaged, a time interval preceding the zero lag is selected to illustrate the phase differences. The waves are constructively interfering (LIN is positive) if they are in-phase, i.e., if the phase difference is $-90° < \Delta\theta < 90°$ and destructively interfering (LIN is negative) if they are out-of-phase, i.e., if the phase difference is $90° < \Delta\theta < 270°$. For the HIGH heat flux events, the composite time mean phase difference varies between 20° and 40° from the mid-troposphere into the stratosphere, while for LOW heat flux events, the composite time mean phase difference varies between 150° and 170° from the mid-troposphere into the stratosphere. The waves are close to neutrally phased in the lower troposphere and are most strongly in or out-of-phase in the stratosphere.

[28] The time evolution of the spatial correlation between $Z^{*\prime}$ and Z^{*}_{c}, at 60°N sheds light on the persistence of the linear interference effect [*Smith et al.*, 2010, 2011]. For HIGH heat flux events, in the stratosphere (100 hPa and above) and troposphere (below 100 hPa), the anomaly correlation remains highly positive for approximately 40 days before the zero lag in both the troposphere and stratosphere (Figures 5b and 5c, solid curves); this effect is dominated by the wave-1 correlation (dashed curves). For corresponding plots of the LOW heat flux composite (Figures 5d and 5e) the behavior is opposite. Thus, both HIGH and LOW heat flux composites exhibit persistent linear interference (constructive and destructive, respectively) preceding the zero lag. The persistent phasing and anti-phasing is what gives rise to the persistent positive and negative LIN flux tendencies illustrated in Figure 3 beginning around a lag of −40 days. (The flux anomalies become statistically significant at around −20 days.) The sudden switch in the sign of

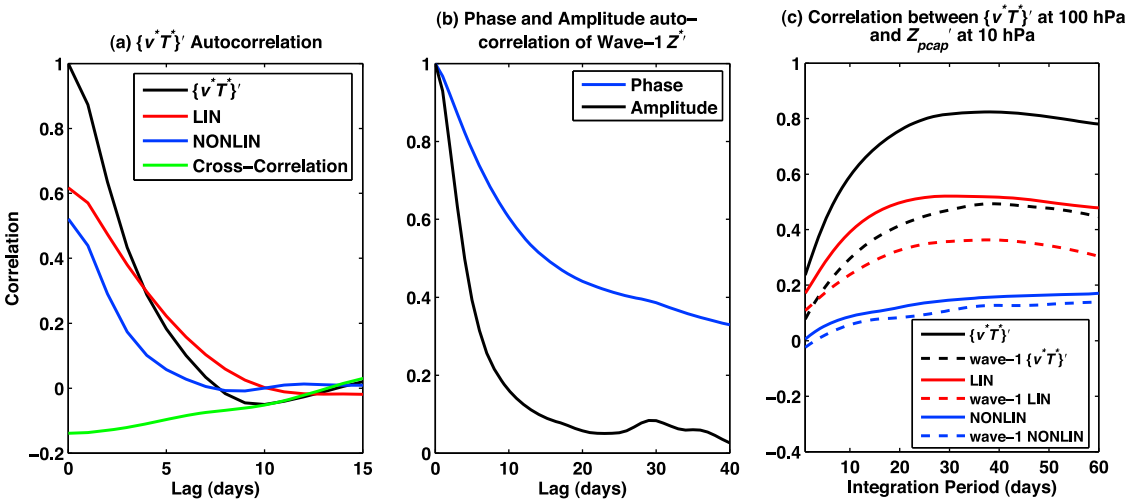

Figure 6. (a) Heat flux anomaly autocorrelations for $\{v^*T^*\}'$ (black line), LIN (red line) and NONLIN (blue line) and the cross-correlation of LIN and NONLIN (green line) at 100 hPa as a function of lag. (b) Amplitude (black line) and phase (blue line) autocorrelations for $Z^{*\prime}$ at 60°N and 100 hPa as a function of lag. (c) Correlation between S(Z_{pcap}') at 10 hPa and $\{v^*T^*\}'$ (black line), LIN (red line) and NONLIN (blue line) at 100 hPa as a function of integration period. Dashed lines show wave-1 component of fluxes.

the anomaly correlation at the zero lag implies a sudden weakening or strengthening of the part of the wave anomaly that projects onto the climatological stationary wave, for the HIGH and LOW heat flux composites, respectively. Approximately 10 days after the zero lag, the anomaly correlations in the troposphere and stratosphere in Figure 5 become uncoupled for both composites and the magnitude of the LIN flux weakens (Figures 3a and 3b).

[29] We stated above that the LIN term includes both phasing and wave amplitude effects. Further analysis demonstrates that there is little coherent change in the wave-1 or wave-2 amplitudes of $Z^{*\prime}$ at 100 hPa and 60°N preceding the zero lag for either the HIGH and LOW heat flux composites (not shown). The one exception is a slight increase in the HIGH heat flux composite mean wave-1 amplitude 5–10 days prior to the zero lag. For HIGH heat flux events, wave-1 amplitude for days [−15, −1] is positively correlated with the NONLIN fluxes ($\rho = 0.6$) but not the LIN fluxes. Thus, the primary process responsible for generating the LIN fluxes in these composites is constructive or destructive interference between $Z^{*\prime}$ and Z^*_c with little contribution from changes in amplitude.

[30] Given that there is little change in amplitude preceding the zero lag of the LOW heat flux composite (this is also true for the LOW LIN and NONLIN composites) and that such a change would not result in *negative* NONLIN anomalies, changes in the baroclinic structure of $Z^{*\prime}$ are likely responsible for the NONLIN flux contribution to the composite shown in Figure 3b. In other words, negative NONLIN fluxes are likely associated with waves whose baroclinicity (anomalous eastward tilt with height) is changing. This has proven difficult to quantify; however, we do find a correlation of 0.3 between the vertical gradient of the phase of the wave-2 component of $Z^{*\prime}$ at 100 hPa and 60°N for days [−15, −1] and the NONLIN fluxes at the zero lag, relating eastward tilted waves to negative NONLIN fluxes and westward tilting waves to positive NONLIN fluxes (not shown). *Perlwitz and Harnik* [2003, 2004], *Shaw and Perlwitz* [2010] and *Shaw et al.* [2010] discuss the occurrence of wave reflection in the NH and find it to be a moderate contribution to stratosphere-troposphere interactions in winter. Wave reflection is characterized by negative $\{v^*T^*\}$. Because the above composites are based on anomalies, $\{v^*T^*\}'$, rather than on the total $\{v^*T^*\}$, there is no direct link between negative NONLIN fluxes and wave reflection. Examination of $\{v^*T^*\}$ indicates that eight of the LOW heat flux events could potentially consist of some wave reflection.

[31] The suggestion from the analysis thus far that LIN fluxes are more persistent than NONLIN fluxes is confirmed in Figure 6a, which shows the autocorrelation of each term in equation (2) at 100 hPa as a function of positive lag (in days) for NDJFM. The lagged autocorrelation of LIN and NONLIN includes the effect of the negative covariance between them resulting in these auto-correlations being less than one at the zero lag. The explicit lagged cross-correlation term is also shown (green line) [*Mudryk and Kushner*, 2011]. The autocorrelation of $\{v^*T^*\}'$ decays relatively quickly. This can be partly attributed to clear differences in the autocorrelation characteristics of the LIN and NONLIN fluxes at lags shorter than 10 days, with the LIN fluxes being more persistent than the NONLIN fluxes. The negative cross-correlation also contributes to the rapid decay of the $\{v^*T^*\}'$ autocorrelation. Thus, linear interference appears to enhance the overall persistence of $\{v^*T^*\}'$ while the NONLIN and cross-correlation components appear to reduce it. Figure 6a is consistent with Figure 2, which shows that the interannual variance of LIN arises primarily from low-frequency waves while that of NONLIN involves significant contributions from other higher-frequency terms in equation (4b).

[32] The persistence of the phasing effect is emphasized in Figure 6b, which shows the autocorrelation function for the phase and amplitude of the anomalous wave-1Z^* for NDJFM at 60°N and 100 hPa. The decorrelation of the phase is considerably slower than that of the amplitude. As discussed

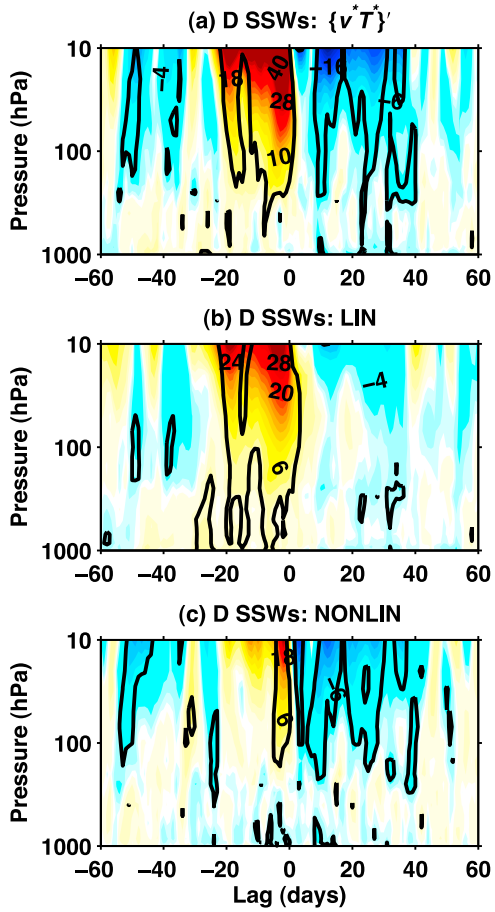

Figure 7. Composite mean daily heat flux anomaly decomposition for Displacement (D) SSWs. (a) $\{v^*T^*\}'$, (b) LIN and (c) NONLIN. Contour interval is 2 mKs^{-1}. Black contour indicates pressures and times for which the composite mean is different from zero at the 95% significance level.

above, the LIN fluxes primarily reflect the phasing between the wave anomaly and the climatological wave while the NONLIN fluxes reflect a complex combination of changes in wave amplitude and baroclinicity. Figure 6b suggests that the persistence of the LIN fluxes arises due to the persistence of the phase of the wave-1Z^* anomaly while the NONLIN fluxes are less persistent due in part to the relatively short autocorrelation timescales of the amplitude of the anomalous wave-1Z^*. Somewhat similar phase and amplitude decorrelation functions exist for wave-2 although they decay approximately twice as quickly as those for wave-1.

[33] Stratospheric NAM anomalies are negatively correlated with 40-day cumulative average $\{v^*T^*\}'$ at 100 hPa [*Polvani and Waugh*, 2004]. Figure 6c shows the correlation between $\{v^*T^*\}'$, LIN and NONLIN and S(Z_{pcap}') at 10 hPa as a function of integration period. It demonstrates that the strongest correlations between $\{v^*T^*\}'$ and the stratospheric circulation occur at integration periods between 30 and 40 days, and that these timescales reflect the timescales of the correlations with the LIN term. The NONLIN correlations are weak for all integration periods. The dashed lines show correlations for the wave-1 component of the fluxes. Although the correlations are weaker, similar correlation characteristics are observed with peak correlations for wave-1 $\{v^*T^*\}'$ and LIN occurring at integration periods between 30 and 40 days and the correlations for NONLIN remaining relatively weak.

[34] In summary, while the LIN term is always important in wave activity events, LIN fluxes are more dominant for the LOW heat flux composite than for the HIGH heat flux composite. LIN flux events are dominated by wave phasing effects rather than wave amplitude effects, and wave-phasing effects control the persistence of the LIN events. Based on this analysis, we propose that identification of persistent anomalous wave-1 phase that constructively or destructively interferes with the climatological stationary wave-1 phase may assist with seasonal prediction of extratropical winter variability, since this persistence might reflect the initiation of a stratosphere-troposphere coupled event.

3.3. Stratospheric Sudden Warming Events and Linear Interference

[35] In this section, the relative contributions of LIN and NONLIN fluxes to SSWs over the period 1958–2009 are investigated. Since SSWs are associated with strong positive wave activity flux anomalies, it is expected that there will be overlap between the HIGH heat flux events of section 3.2 and SSW events. Indeed, of the 19 SSWs that occurred in the period 1979–2009 in Table 1, 12 correspond to HIGH heat flux events according to the classification of section 3.2 because these SSWs were the largest $\{v^*T^*\}'$ events in their respective years. The remaining 7 SSWs of that period were not the strongest positive $\{v^*T^*\}'$ events in their respective seasons.

[36] *Charlton and Polvani* [2007] demonstrate that there are two distinct classes of SSWs: displacement (D) SSWs that are preceded by relatively weak and persistent $\{v^*T^*\}'$ and dominated by wave-1 $\{v^*T^*\}'$, and split (S) SSWs that are preceded by relatively strong and pulse-like $\{v^*T^*\}'$ and dominated by wave-2 $\{v^*T^*\}'$. The analysis of section 3.2 suggests that D SSWs correspond to LIN events and that S SSWs correspond to NONLIN events. To support this claim, the composite mean $\{v^*T^*\}'$, LIN, and NONLIN are plotted for the 20 D events (Figure 7) and the 13 S events (Figure 8) that occurred during the 1958–2009 period. In Figures 7 and 8, daily rather than 40-day averaged $\{v^*T^*\}'$ are used in order to directly compare this analysis with other published work on SSWs [*Charlton and Polvani*, 2007; *Nishii et al.*, 2009; *Cohen and Jones*, 2011]. D and S events are clearly distinguishable by the nature of $\{v^*T^*\}'$ preceding them; D events are preceded by a steady increase in LIN heat fluxes (primarily wave-1 (not shown); Figure 7b) and S events are preceded by a pulse of NONLIN heat fluxes (primarily wave-2 (not shown); Figure 8c). Figure 7b also demonstrates the robust persistence of the LIN fluxes preceding the D events relative to the NONLIN fluxes preceding the S events in Figure 8c. Figures 7 and 8 also demonstrate different processes driving the suppression of wave activity flux following the different types of SSW events. D events are followed by a suppression of primarily NONLIN fluxes (Figure 7c) while S events are followed by strong negative LIN fluxes (i.e., strong negative interference; Figure 8b). Thus, the $\{v^*T^*\}'$ decomposition provides

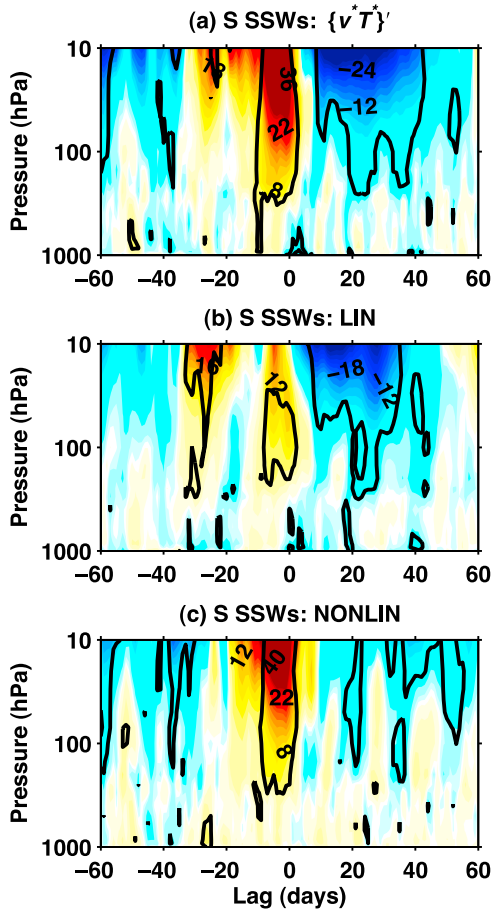

Figure 8. Composite mean daily heat flux anomaly decomposition for Split (S) SSWs. (a) $\{v^*T^*\}'$, (b) LIN and (c) NONLIN. Contour interval is 2 mKs^{-1}. Black contour indicates pressures and times for which the composite mean is different from zero at the 95% significance level.

evidence for complementary processes controlling displacement and split SSW events.

[37] These results are partially consistent with *Martius et al.*'s [2009] description of wave-1 constructive interference preceding displacement events but differ somewhat from their conclusion that split SSWs are associated with constructive interference of wave-2. Instead, this result suggests that instrinsic wave activity associated with wave anomalies themselves is the primary driver of split SSWs. There is some evidence in Figure 8b that there may be a preconditioning of the vortex due to positive LIN fluxes at a lag of −30 days; however, these positive LIN fluxes are partially canceled by negative NONLIN fluxes. It is notable that *Cohen and Jones* [2011] show that displacement events are preceded by a zonally asymmetric tropospheric circulation pattern that is consistent with the enhancement of LIN fluxes preceding these events.

3.4. Comparison Between Northern and Southern Hemisphere

[38] Figure 9 shows the monthly $\{v^*T^*\}$ variance decomposition for the SH using equation (3). The total variance grows slowly over the austral autumn and winter, but there is a doubling in the variance from August to September with a peak in October (black line). Late winter and spring (September–December) are when stratosphere-troposphere interactions are most frequent in the SH [*Thompson et al.*, 2005]. In late spring and summer, the variance decreases sharply, reaching a minimum in February [see also *Randel*, 1988]. From August to November, the variance of the LIN fluxes (red line) is the largest contribution to the total variance. The variance of the NONLIN fluxes (blue line) for the most part is larger from December to July. In June, the larger LIN contribution to the variance reflects the weaker stratospheric winds in the early winter season allowing for greater amplitude and vertical propagation of the stationary wavefield than in July [*Plumb*, 1989; *Yoden*, 1990; *Scott and Haynes*, 2002]. The contribution from the covariance between LIN and NONLIN (green line) is typically negative although LIN and NONLIN are not significantly correlated and the covariance is weaker in the SH than the NH.

[39] As in the NH, the LIN fluxes primarily consist of low-frequency waves (red dashed line in Figure 9), while the NONLIN fluxes consist of both low- and high-frequency wave contributions (blue dashed line in Figure 9). Thus, in general, the SH wave activity flux is dominated by low-frequency LIN fluxes, similar to the NH.

[40] How does the relative contribution of LIN to the $\{v^*T^*\}$ variance carry over to extreme events in the SH? Using the maximum and minimum composite method, 29 HIGH heat flux events and 30 LOW heat flux events are identified in the period 1979–2009 (Table 1; the HIGH heat flux event of 2002 was a major SSW; this event is excluded). The mean date of the HIGH heat flux events is November 10th with a standard

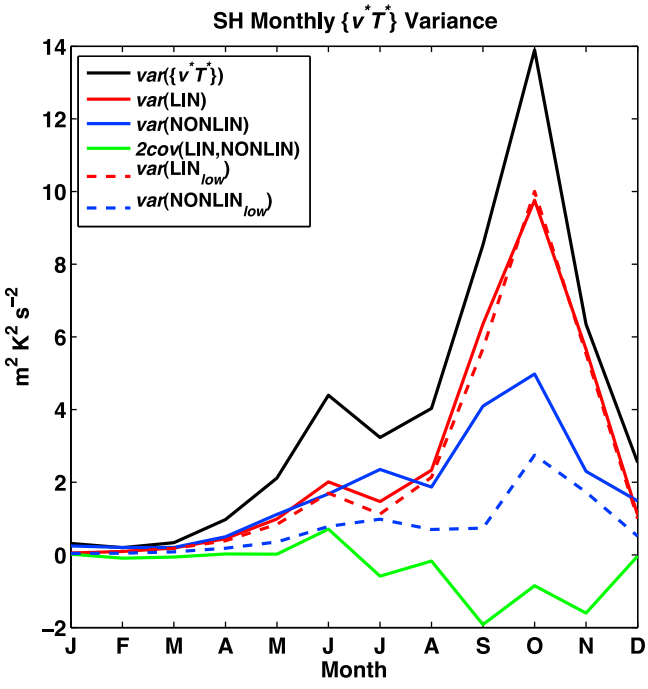

Figure 9. Monthly interannual $\{v^*T^*\}$ variance decomposition at 100 hPa averaged over 40–80°S (see equations (3) and (4b)). Subscript "low" indicates fluxes that were calculated using 11-day low-pass filtered wavefields.

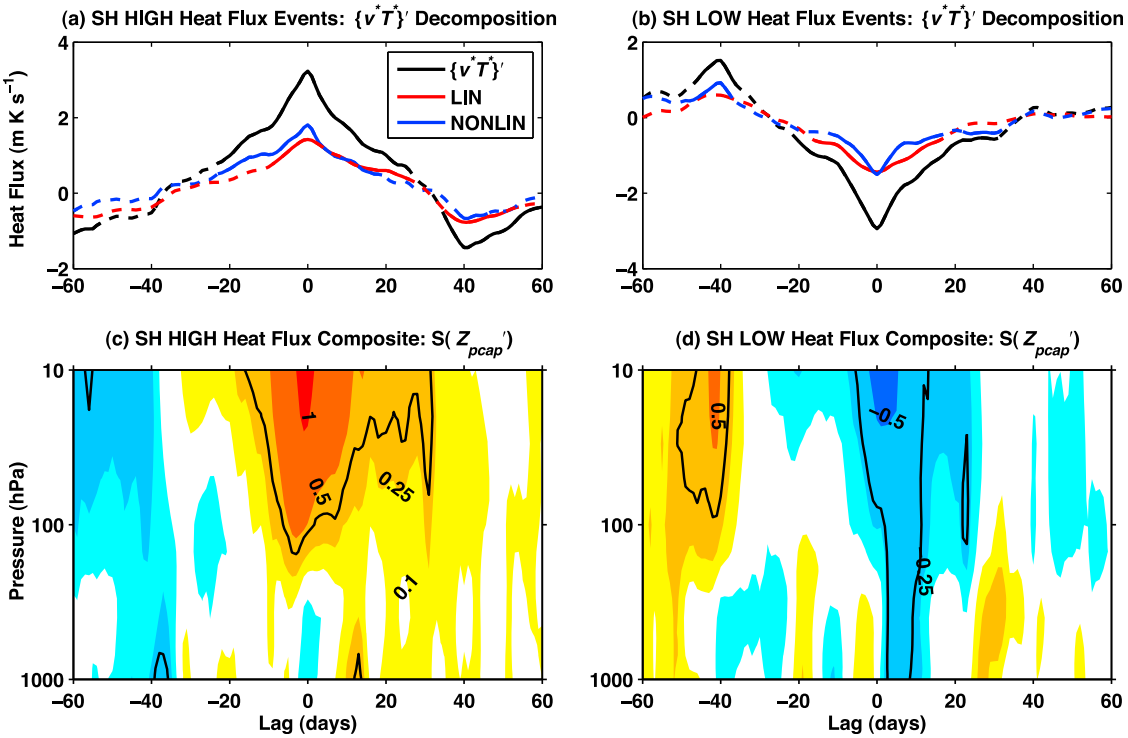

Figure 10. Composite mean 40-day averaged heat flux anomaly decomposition at 100 hPa; $\{v^*T^*\}'$ (black line), LIN (red line) and NONLIN (blue line) for SH (a) HIGH and (b) LOW heat flux events. Solid sections of the lines indicate times for which the composite mean is different from zero at the 95% significance level. Composite mean S(Z_{pcap}') for SH (c) HIGH and (d) LOW heat flux events. Contour interval is [−1.5 −1 −0.5 −0.25 −0.1 0.1 0.25 0.5 1 1.5]. Black contour indicates pressures and times for which the composite mean is different from zero at the 95% significance level.

deviation of 66 days; the mean date of the LOW heat flux events is October 21st with a standard deviation of 73 days. Similar to Figure 3, Figures 10a and 10b show composites for $\{v^*T^*\}'$, LIN and NONLIN for HIGH and LOW events in the SH, respectively (the convention used is that positive $\{v^*T^*\}'$ corresponds to poleward $\{v^*T^*\}'$). Unlike in the NH, for both composites, we see that the NONLIN fluxes contribute slightly more to $\{v^*T^*\}'$ than the LIN fluxes. As in the NH, the LIN fluxes increase linearly toward the zero lag while the NONLIN fluxes increase rapidly very close to the zero lag. The corresponding S(Z_{pcap}') in Figures 10c and 10d show robust negative and positive stratospheric Southern Annular Mode (SAM) signatures, respectively. The composite mean $\{v^*T^*\}'$ for both composites is slightly weaker in the SH than the NH, which is linked to the weaker S(Z_{pcap}') and stratosphere-troposphere coupling in the SH.

[41] As was done for the NH, complementary composites of maximum and minimum LIN and NONLIN fluxes are constructed (Table 1). While in the NH there were more LIN events that coincided with the HIGH and LOW heat flux events, in the SH there are more NONLIN events that coincide with HIGH and LOW heat flux events. Specifically, there are 17 (12) HIGH (LOW) NONLIN and 6 (7) HIGH (LOW) LIN events. Two of the 17 HIGH NONLIN events are also HIGH LIN vortex events.

[42] The linear interference diagnostics shown in Figure 5 for the NH are very similar for the SH (not shown). The main differences include slightly weaker-magnitude anomaly correlations between $Z^{*\prime}$ and Z^*_c preceding the zero lag, particularly in the troposphere, for both the HIGH and LOW heat flux composites. This is likely due to the less stationary nature of long waves in the SH [*Manney et al.*, 1991]. However, the SH also exhibits persistent constructive and destructive interference of up to 30 days preceding the zero lag for HIGH and LOW heat flux events, respectively. As in the NH, it is found that the LIN fluxes are primarily wave-1 while the NONLIN fluxes consist of an equal contribution from wave-2. Examination of the full heat fluxes shows that there are potentially eight events in the SH LOW heat flux composite that consist of some wave reflection, i.e., the full heat fluxes preceding the zero lag are negative.

[43] Comparing our composite method to the threshold method of *Polvani and Waugh* [2004] reveals that the main features shown in Figure 10 are representative over a range of threshold values (see section 2). A notable difference between the SH and NH at large negative threshold values is the dominance of the NONLIN fluxes in the SH, illustrating greater anomalously eastward-tilting waves and wave reflection in the SH [*Shaw et al.* 2010].

[44] In summary, although the stationary wavefield is markedly weaker in the SH compared to the NH, LIN fluxes, which are dominated by phasing effects, and NONLIN fluxes, which are dominated by variability in the vertical tilt of the wave anomalies contribute roughly equally to SH polar vortex variability. In terms of anomalously eastward

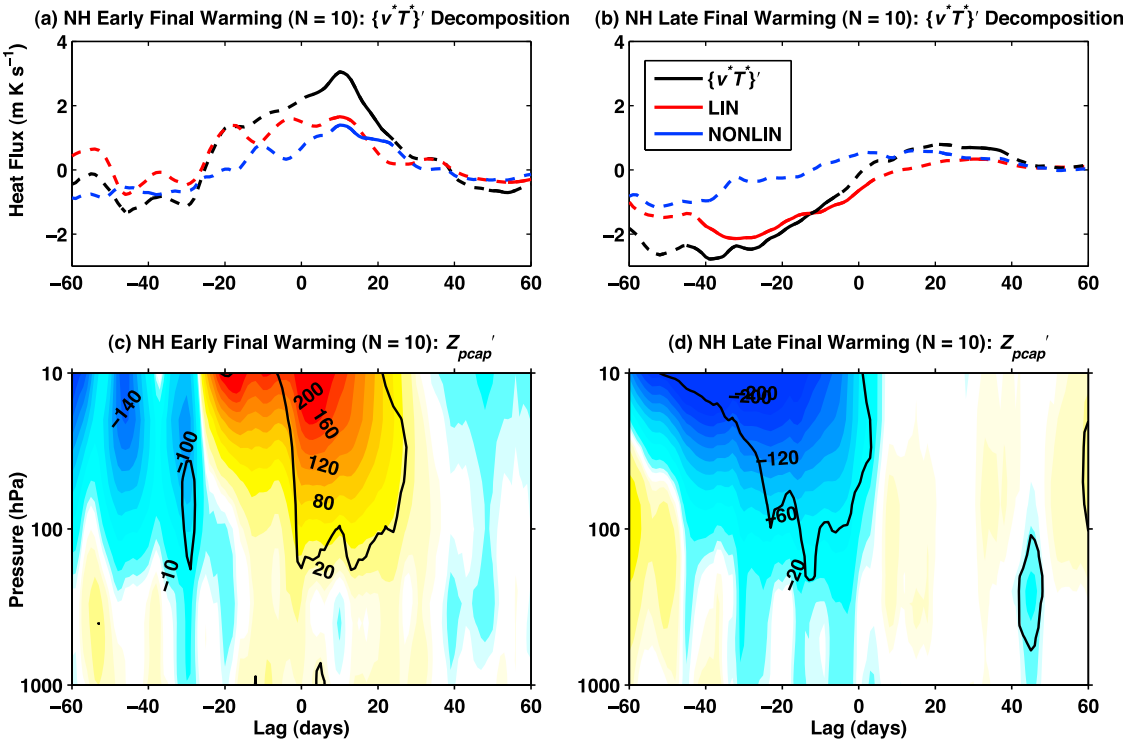

Figure 11. Composite mean 40-day averaged heat flux anomaly decomposition at 100 hPa; $\{v^*T^*\}'$ (black line), LIN (red line) and NONLIN (blue line) for (a) "early" and (b) "late" NH SFWs. Solid sections of the lines indicate times for which the composite mean is different from zero at the 95% significance level. Composite mean Z_{pcap}' for (c) "early" and (d) "late" NH SFWs. Contour interval is […, −40, −20, −10, −5, 5, 10, 20, 40,…]. Black contour indicates pressures and times for which the composite mean is different from zero at the 95% significance level.

tilting waves, the SH and NH differ in that while in the NH, negative NONLIN fluxes do contribute to strong vortex events, they are substantially weaker and do not play as important a role as in the SH.

3.5. Stratospheric Final Warmings and Linear Interference

[45] To conclude the discussion of linear interference in stratosphere-troposphere interactions, we diagnose the $\{v^*T^*\}'$ decomposition associated with "early" and "late" season stratospheric final warmings (SFWs). As for the previous examples, we find that the variability in the timing of SFWs is associated with significant contributions from linear interference effects.

[46] As mentioned in section 2, for this analysis, no linear trends are removed from the data. This heuristic approach is taken because there has been a pronounced trend in the timing of the SH SFW: the delayed breakdown of the SH polar vortex in spring is a well-known consequence of the Antarctic ozone hole [*Black and McDaniel*, 2007b; *Eyring et al.*, 2010, chapter 4; *Thompson et al.*, 2011]. The mean date of NH SFW onset is April 20th with a standard deviation of 18 days and the mean date of SH SFW onset is December 7th with a standard deviation of 12 days. Of the 30 SFWs in both the NH and SH, the 10 earliest and 10 latest are chosen for "early" and "late" composites of SFWs. The mean dates of "early" and "late" NH SFW onset are April 1st with a standard deviation of 10 days and May 10th with a standard deviation of 9 days. The corresponding dates in the SH are November 23rd with a standard deviation of 4 days and December 19th with a standard deviation of 6 days. As expected, in the SH the late events are typically from the latter part of the climate record and the early events from the earlier part of the record. In the NH the events are randomly distributed across the record.

[47] Figures 11a and 11c and 11b and 11d show the composite mean 40-day averaged $\{v^*T^*\}'$ (black line), LIN (red line) and NONLIN (blue line) flux anomalies and Z_{pcap}' for "early" and "late" NH SFWs, respectively. "Early" SFWs are associated with weak and generally marginally significant positive $\{v^*T^*\}'$ after the mean date of the SFW (lag 0). Of the 10 "early" SFWs, six are predominantly LIN events and only one is clearly a NONLIN event. "Late" SFWs, on the other hand, are associated with primarily negative LIN anomalies (Figure 11b). Thus delayed springtime transitions in the stratosphere are associated with a wave anomaly field that cancels the stationary wave pattern, while early transitions are not associated with a clear pattern of behavior.

[48] The situation is somewhat more interesting in the SH (Figure 12), where the timing of the springtime transition is dominated by linear interference effects: LIN flux anomalies preceding the zero lag are positive for the "early" composite and negative for the "late" composite. Figure 12 has an implication for simulation of the SH stratosphere in climate models. The SFW in chemistry climate models (CCMs) tends to occur later than observed; this bias has been attributed to

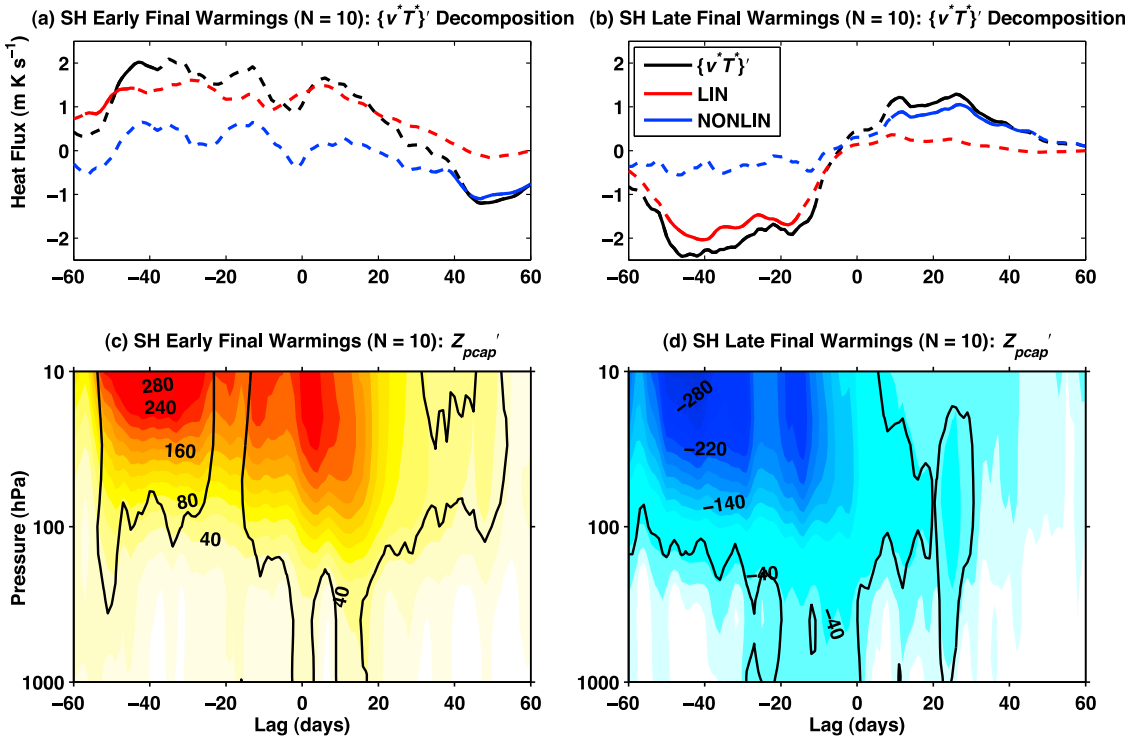

Figure 12. Composite mean 40-day averaged heat flux anomaly decomposition at 100 hPa; $\{v^*T^*\}'$ (black line), LIN (red line) and NONLIN (blue line) for (a) "early" and (b) "late" SH SFWs. Solid sections of the lines indicate times for which the composite mean is different from zero at the 95% significance level. Composite mean $Z_{pcap}{}'$ for (c) "early" and (d) "late" SH SFWs. Contour interval is […, −40, −20, −10, 10, 20, 40,…]. Black contour indicates pressures and times for which the composite mean is different from zero at the 95% significance level.

stationary wave biases and poorly simulated gravity wave drag effects [*Hurwitz et al.*, 2010; *McLandress et al.*, 2012]. The current analysis suggests that discrepancies in the phasing of the wave anomalies with respect to the climatological stationary wave could also play a role in this bias.

4. Conclusions

[49] This paper has examined the role of linear interference in initiating NH and SH stratosphere-troposphere interactions using a decomposition of interannual variability in the vertical wave activity flux in to terms LIN and NONLIN that are linear and quadratic in wave anomalies. In both hemispheres, LIN fluxes are dominated by contributions from low-frequency waves and tend to partially cancel NONLIN fluxes (Figures 2 and 9). In the NH, anomalously high heat flux events consist of a greater contribution from NONLIN fluxes than anomalously low heat flux events, reflecting in part the positive and negative skew of the NONLIN and LIN flux distributions. Linear interference diagnostics demonstrate that the time evolution of the phasing of the wave-1 anomaly with the wave-1 climatological wave explains most of the time evolution of the spatial correlation of the full wave anomaly with the climatological wavefield. In addition, phasing throughout the depth of the troposphere and stratosphere appears necessary in order to establish coherent LIN fluxes. Constructive or destructive interference between wave anomalies and the climatological wave begins approximately 40 days before the anomalous heat flux event. The wave-1 phase appears to be a relatively persistent variable with a multiple week timescale that might be exploited for seasonal prediction. This paper has also shown that displacement stratospheric sudden warming (SSW) events are predominantly LIN events and that split SSWs are predominantly NONLIN events. Due to the persistence of anomalous wave patterns preceding LIN events, the work suggests that displacement SSWs may be potentially predictable.

[50] LIN flux terms play a surprisingly large role in SH vertical wave activity flux variability, despite the relatively weak stationary wavefield (Figure 9). SH anomalously high and low heat flux events consist of roughly equal contributions from LIN and NONLIN fluxes, although there are more strong NONLIN events in the SH composites relative to the NH. As in the NH, linear interference diagnostics show that constructive and destructive interference begins roughly 30 days before the anomalous heat flux events.

[51] Finally, a comparison of "early" and "late" stratospheric final warming composites in both the NH and SH reveals that these events are associated with weak heat flux anomalies consisting of a substantial contribution from LIN, particularly in the SH. Thus interactions involving the stationary wavefield can still affect the zonal mean circulation even as the stationary wavefield is being suppressed during the transition from westerly to easterly flow.

[52] At this point we have not developed a hypothesis as to why linear interference operates so strongly in wave

driving from the troposphere to stratosphere and, as such, this work leaves several open questions. Is there a mechanism that couples the wave phase to the zonal mean circulation? What sets the ∼40-day persistence time scale of linear interference? Do the LIN events identified here involve traveling waves that transition into and out of phase with the climatological stationary wavefield, or do they involve a growing and decaying stationary wave pattern? Answers to these questions may improve our understanding of wave-mean flow dynamics in the presence of a zonally asymmetric background flow.

[53] In summary, as *DeWeaver and Nigam* [2000a] demonstrate for momentum fluxes (horizontal wave activity fluxes) and zonal mean variability in the troposphere, this paper demonstrates that linear interference is an integral part of heat flux (vertical wave activity flux) variability and zonal mean variability in the stratosphere, and, consequently, the coupled variability of the stratosphere and troposphere. Taken together, the present study and *DeWeaver and Nigam* [2000a] demonstrate that interactions between anomalies and the large-scale zonally asymmetric circulation appear to be vitally important to Annular Mode dynamics in both the troposphere and stratosphere. Future work includes establishing a better understanding of how the persistence of the LIN fluxes relates to the timescales of the Annular Modes. In addition, the extent to which linear interference plays a role in tropospheric SAM variability has yet to be investigated.

[54] **Acknowledgments.** The authors would like to thank W. R. Peltier, T. G. Shepherd, K. Strong and I. Simpson for their helpful comments. We would also like to acknowledge the support of the Natural Science and Engineering Research Council of Canada and the Canadian Foundation for Climate and Atmospheric Sciences (grant 506).

References

Ayarzagüena, B., and E. Serrano (2009), Monthly characterization of the tropospheric circulation over the Euro-Atlantic area in relation with the timing of stratospheric final warmings, *J. Clim.*, *22*, 6313–6324, doi:10.1175/2009JCLI2913.1.

Baldwin, M. P., and T. P. Dunkerton (2001), Stratospheric harbingers of anomalous weather regimes, *Science*, *294*, 581–584, doi:10.1126/science.1063315.

Baldwin, M. P., and D. W. J. Thompson (2009), A critical comparison of stratosphere-troposphere coupling indices, *Q. J. R. Meteorol. Soc.*, *135*, 1661–1672, doi:10.1002/qj.479.

Black, R. X., and B. A. McDaniel (2007a), The dynamics of Northern Hemisphere stratospheric final warming events, *J. Atmos. Sci.*, *64*, 2932–2946, doi:10.1175/JAS3981.1.

Black, R. X., and B. A. McDaniel (2007b), Interannual variability in the Southern Hemisphere circulation organized by stratospheric final warming events, *J. Atmos. Sci.*, *64*, 2968–2974, doi:10.1175/JAS3979.1.

Black, R. X., B. A. McDaniel, and W. A. Robinson (2006), Stratosphere-troposphere coupling during spring onset, *J. Clim.*, *19*, 4891–4901, doi:10.1175/JCLI3907.1.

Branstator, G. (1992), The maintenance of low-frequency atmospheric anomalies, *J. Atmos. Sci.*, *49*, 1924–1946, doi:10.1175/1520-0469(1992)049<1924:TMOLFA>2.0.CO;2.

Butler, A. H., and L. M. Polvani (2011), El Niño, La Niña, and stratospheric sudden warmings: A re-evaluation in light of the observational record, *Geophys. Res. Lett.*, *38*, L13807, doi:10.1029/2011GL048084.

Cagnazzo, C., and E. Manzini (2009), Impact of the stratosphere on the winter tropospheric teleconnections between ENSO and the North Atlantic and European region, *J. Clim.*, *22*, 1223–1238, doi:10.1175/2008JCLI2549.1.

Charlton, A. J., and L. M. Polvani (2007), A new look at stratospheric sudden warmings. Part I. Climatology and modeling benchmarks, *J. Clim.*, *20*, 449–469, doi:10.1175/JCLI3996.1.

Charlton, A. J., L. M. Polvani, J. Perlwitz, F. Sassi, E. Manzini, S. Pawson, J. E. Nielsen, K. Shibata, and D. Rind (2007), A new look at stratospheric sudden warmings. Part II. Evaluation of numerical model simulations, *J. Clim.*, *20*, 470–488, doi:10.1175/JCLI3994.1.

Cohen, J., and J. Jones (2011), Tropospheric precursors and stratospheric warmings, *J. Clim.*, *24*, 6562–6572, doi:10.1175/2011JCLI4160.1.

Cohen, J., D. Salstein, and K. Saito (2002), A dynamical framework to understand and predict the major Northern Hemisphere mode, *Geophys. Res. Lett.*, *29*(10), 1412, doi:10.1029/2001GL014117.

de la Torre, L., R. R. Garcia, D. Barriopedro, and A. Chandran (2012), Climatology and characteristics of stratospheric sudden warmings in the Whole Atmosphere Community Climate Model, *J. Geophys. Res.*, *117*, D04110, doi:10.1029/2011JD016840.

DeWeaver, E., and S. Nigam (2000a), Do stationary waves drive the zonal-mean jet anomalies of the northern winter?, *J. Clim.*, *13*, 2160–2176, doi:10.1175/1520-0442(2000)013<2160:DSWDTZ>2.0.CO;2.

DeWeaver, E., and S. Nigam (2000b), Zonal-eddy dynamics of the North Atlantic Oscillation, *J. Clim.*, *13*, 3893–3914, doi:10.1175/1520-0442(2000)013<3893:ZEDOTN>2.0.CO;2.

Eyring, V., T. G. Shepherd, and D. W. Waugh (Eds.) (2010), Stratospheric processes and their role in climate. SPARC report on the evaluation of chemistry-climate models, *SPARC Rep. 5*, World Clim. Res. Programme, Geneva, Switzerland.

Fletcher, C. G., and P. J. Kushner (2011), The role of linear interference in the annular mode response to tropical SST forcing, *J. Clim.*, *24*, 778–794, doi:10.1175/2010JCLI3735.1.

Garfinkel, C. I., D. L. Hartmann, and F. Sassi (2010), Tropospheric precursors of anomalous Northern Hemisphere stratospheric polar vortices, *J. Clim.*, *23*, 3292–3299, doi:10.1175/2010JCLI3010.1.

Hardiman, S. C., et al. (2011), Improved predictability of the troposphere NAO using stratosphere final warmings, *J. Geophys. Res.*, *116*, D18113, doi:10.1029/2011JD015914.

Hurwitz, M. M., P. A. Newman, F. Li, L. D. Oman, O. Morgenstern, P. Braesicke, and J. A. Pyle (2010), Assessment of the breakup of the Antarctic polar vortex in two new chemistry-climate models, *J. Geophys. Res.*, *115*, D07105, doi:10.1029/2009JD012788.

Ineson, S., and A. A. Scaife (2009), The role of the stratosphere in the European response to El Niño, *Nat. Geosci.*, *2*, 32–36, doi:10.1038/ngeo381.

Kalnay, E., et al. (1996), The NCEP/NCAR 40-year reanalysis project, *Bull. Am. Meteorol. Soc.*, *77*, 437–471.

Kistler, R., et al. (2001), The NCEP-NCAR 50-year reanalysis: Monthly means CD-ROM and documentation, *Bull. Am. Meteorol. Soc.*, *82*, 247–267, doi:10.1175/1520-0477(2001)082<0247:TNNYRM>2.3.CO;2.

Kodera, K., M. Chiba, H. Koide, A. Kitoh, and Y. Nikaidou (1996), Interannual variability of the winter stratosphere and troposphere in the Northern Hemisphere, *J. Meteorol. Soc. Jpn.*, *74*, 365–382.

Kolstad, E. W., and A. J. Charlton-Perez (2010), Observed and simulated precursors of stratospheric polar vortex anomalies in the Northern Hemisphere, *Clim. Dyn.*, *37*, 1443–1456, doi:10.1007/s00382-010-0919-7.

Limpasuvan, V., D. W. J. Thompson, and D. L. Hartmann (2004), The life cycle of the Northern Hemisphere sudden stratospheric warmings, *J. Clim.*, *17*, 2584–2596, doi:10.1175/1520-0442(2004)017<2584:TLCOTN>2.0.CO;2.

Manney, G. L., J. D. Farrara, and C. R. Mechoso (1991), The behavior of wave 2 in the Southern Hemisphere stratosphere during late winter and early spring, *J. Atmos. Sci.*, *48*, 976–998, doi:10.1175/1520-0469(1991)048<0976:TBOWIT>2.0.CO;2.

Martius, O., L. M. Polvani, and H. C. Davies (2009), Blocking precursors to stratospheric sudden warming events, *Geophys. Res. Lett.*, *36*, L14806, doi:10.1029/2009GL038776.

Matthewman, N. J., J. G. Esler, A. J. Charlton-Perez, and L. M. Polvani (2009), A new look at stratospheric sudden warmings. Part III. Polar vortex evolution and vertical structure, *J. Clim.*, *22*, 1566–1585, doi:10.1175/2008JCLI2365.1.

McLandress, C., T. G. Shepherd, S. Polavarapu, and S. R. Beagley (2012), Is missing orographic gravity wave drag near 60°S the cause of the stratospheric zonal wind biases in chemistry-climate models?, *J. Atmos. Sci.*, *69*, 802–818, doi:10.1175/JAS-D-11-0159.1.

Mudryk, L. R., and P. J. Kushner (2011), A method to diagnose sources of annular mode timescales, *J. Geophys. Res.*, *116*, D14114, doi:10.1029/2010JD015291.

Newman, P. A., E. R. Nash, and J. E. Rosenfield (2001), What controls the temperature of the Arctic stratosphere during the spring?, *J. Geophys. Res.*, *106*(D17), 19,999–20,010, doi:10.1029/2000JD000061.

Nishii, K., H. Nakamura, and T. Miyasaka (2009), Modulations in the planetary wave field induced by upward-propagating Rossby wave packets prior to stratospheric sudden warming events: A case-study, *Q. J. R. Meteorol. Soc.*, *135*, 39–52, doi:10.1002/qj.359.

Nishii, K., H. Nakamura, and Y. J. Orsolini (2010), Cooling of the wintertime Arctic stratosphere induced by the western Pacific teleconnection pattern, *Geophys. Res. Lett.*, *37*, L13805, doi:10.1029/2010GL043551.

Nishii, K., H. Nakamura, and Y. J. Orsolini (2011), Geographical dependence observed in blocking high influence on the stratospheric variability

through enhancement and suppression of upward planetary-wave propagation, *J. Clim.*, *24*, 6408–6423, doi:10.1175/JCLI-D-10-05021.1.

Perlwitz, J., and N. Harnik (2003), Observational evidence of a stratospheric influence on the troposphere by planetary wave reflection, *J. Clim.*, *16*, 3011–3026, doi:10.1175/1520-0442(2003)016<3011:OEOASI>2.0.CO;2.

Perlwitz, J., and N. Harnik (2004), Downward coupling between the stratosphere and troposphere: The relative roles of wave and zonal mean processes, *J. Clim.*, *17*, 4902–4909, doi:10.1175/JCLI-3247.1.

Plumb, R. A. (1989), On the seasonal cycle of stratospheric planetary waves, *Pure Appl. Geophys.*, *130*, 233–242, doi:10.1007/BF00874457.

Polvani, L. M., and D. W. Waugh (2004), Upward wave activity flux as precursor to extreme stratospheric events and subsequent anomalous surface weather regimes, *J. Clim.*, *17*, 3548–3554.

Randel, W. J. (1988), The seasonal evolution of planetary waves in the Southern Hemisphere stratosphere and troposphere, *Q. J. R. Meteorol. Soc.*, *114*, 1385–1409, doi:10.1002/qj.49711448403.

Salby, M. L., and P. F. Callaghan (2007), Influence of planetary wave activity on stratospheric final warming and spring ozone, *J. Geophys. Res.*, *112*, D20111, doi:10.1029/2006JD007536.

Scott, R. K., and P. H. Haynes (2002), The seasonal cycle of planetary waves in the winter stratosphere. *J. Atmos. Sci.*, *59*, 803–822.

Shaw, T. A., and J. Perlwitz (2010), The impact of stratospheric model configuration on planetary scale waves in Northern Hemisphere winter, *J. Clim.*, *23*, 3369–3389, doi:10.1175/2010JCLI3438.1.

Shaw, T. A., J. Perlwitz, and N. Harnik (2010), Downward wave coupling between the statosphere and troposphere: The importance of meridional wave guiding and comparison with zonal-mean coupling, *J. Clim.*, *23*, 6365–6381, doi:10.1175/2010JCLI3804.1.

Smith, K. L. (2011), Eurasian snow cover and the role of linear interference in stratosphere-troposphere interactions, PhD thesis. Univ. of Toronto, Toronto, Ont., Canada.

Smith, K. L., C. G. Fletcher, and P. J. Kushner (2010), The role of linear interference in the Annular Mode response to extratropical surface forcings, *J. Clim.*, *23*, 6036–6050, doi:10.1175/2010JCLI3606.1.

Smith, K. L., P. J. Kushner, and J. Cohen (2011), The role of linear interference in Northern Annular Mode variability associated with Eurasian snow cover extent, *J. Clim.*, *24*, 6185–6202, doi:10.1175/JCLI-D-11-00055.1.

Taguchi, M. (2008), Is there a statistical connection between stratospheric sudden warming and tropospheric blocking events?, *J. Atmos. Sci.*, *65*, 1442–1454, doi:10.1175/2007JAS2363.1.

Taguchi, M., and S. Yoden (2002), Internal interannual variability of the troposphere-stratosphere coupled system in a simple global circulation model. Part I: Parameter sweep experiment, *J. Atmos. Sci.*, *59*, 3021–3036, doi:10.1175/1520-0469(2002)059<3021:IIVOTT>2.0.CO;2.

Thompson, D. W. J., M. P. Baldwin, and S. Solomon (2005), Stratosphere-troposphere coupling in the Southern Hemisphere, *J. Atmos. Sci.*, *62*, 708–715, doi:10.1175/JAS-3321.1.

Thompson, D. W. J., S. Solomon, P. J. Kushner, M. H. England, K. M. Grise, and D. J. Karoly (2011), Signatures of the Antarctic ozone hole in Southern Hemisphere surface climate change, *Nat. Geosci.*, *4*, 741–749, doi:10.1038/ngeo1296.

Trenberth, K. E., and D. P. Stepaniak (2003), Covariability of components of poleward atmospheric energy transports on seasonal and interannual timescales, *J. Clim.*, *16*, 3691–3705, doi:10.1175/1520-0442(2003)016<3691:COCOPA>2.0.CO;2.

Watanabe, M., and T. Nitta (1998), Relative impacts of snow and sea surface temperature anomalies on an extreme phase in the winter atmospheric circulation, *J. Clim.*, *11*, 2837–2857, doi:10.1175/1520-0442(1998)011<2837:RIOSAS>2.0.CO;2.

Weickmann, K. M., and P. D. Sardeshmukh (1994), The atmospheric angular momentum cycle associated with a Madden-Julian oscillation, *J. Atmos. Sci.*, *51*, 3194–3208, doi:10.1175/1520-0469(1994)051<3194:TAAMCA>2.0.CO;2.

Woollings, T. J., A. J. Charlton-Perez, S. Ineson, A. G. Marshall, and G. Masato (2010), Associations between stratospheric variability and tropospheric blocking, *J. Geophys. Res.*, *115*, D06108, doi:10.1029/2009JD012742.

Yoden, S. (1990), An illustrative model of seasonal and interannual variations of the stratospheric circulation, *J. Atmos. Sci.*, *47*, 1845–1853, doi:10.1175/1520-0469(1990)047<1845:AIMOSA>2.0.CO;2.